JOURNAL OF COMPUTATIONAL PHYSICS 121, 51–65 (1995)

A Simple Riemann Solver and High-Order Godunov Schemes for Hyperbolic Systems of Conservation Laws

WENLONG DAI AND PAUL R. WOODWARD

School of Physics and Astronomy, Supercomputer Institute, Army High Performance Computing Research Center, University of Minnesota, 1100 Washington Avenue South, Minneapolis, Minnesota 55415

Received September 6, 1994; revised January 31, 1995

A simple approximate Riemann solver for hyperbolic systems of conservation laws is developed for its use in Godunov schemes. The solver is based on characteristic formulations and is illustrated through Euler and ideal magnetohydrodynamical (MHD) equations. The procedure of a high-order Godunov scheme incorporated with the Riemann solver for one-dimensional hyperbolic systems of conservation laws is described in detail. The correctness of the scheme is shown by comparison with the piecewise parabolic method for Euler equations and by comparison with exact solutions of Riemann problems for ideal MHD equations. The robustness of the scheme is demonstrated through numerical examples involving more than one strong shock at the same time. It is shown that the scheme offers the principle advantages of Godunov schemes: robust operation in the presence of strong waves, thin shock fronts, thin contact and slip surface discontinuities.

1. INTRODUCTION

It is well known that a first-order accurate scheme for a hyperbolic system of conservation laws will give numerical results which are very smeared in regions near discontinuities. The reason for the smearing is the large amount of numerical viscosity in a first-order accurate scheme. If a standard second-order scheme is used, the numerical viscosity will be reduced, but large oscillations will be introduced in numerical solutions near discontinuities.

During the last 20 years, a lot of effort has been put on the development of effective numerical schemes for hyperbolic systems of conservation laws. The result of the effort is the generation of modern numerical methods for conservation laws (e.g., [1–15]). Among them, Godunov schemes have been particularly efficient for shock problems. Godunov [1] supposed that initial data could be replaced by a set of piecewise constant states with discontinuities and he used exact solutions of Riemann problems to advance the piecewise constant data. The first major extension to the Godunov's scheme was made by Van Leer [5] in his MUSCL scheme which used a Riemann solver to advance piecewise linear data, introduced a monotonicity constraint, and applied a smart artificial viscosity. Based on a robust Riemann solver, the piecewise parabolic method (PPM) [8, 11] was developed for Euler equations. The principal advantages of these schemes are robust operation in the presence of strong waves, thin shock fronts with little attendant noise generation, and thin contact and slip surface discontinuities.

Although approximate Riemann solvers used in current numerical schemes for Euler equations may be fairly simple, such as the solver in [6, 11], but it is not true for more complicated systems of conservation laws. For example, Riemann solvers for ideal MHD equations are quite complicated [16–19], and the complexity of the Riemann solver is determined by the hyperbolic system itself. Brio and Wu [16] applied Roe's method [6] to ideal MHD equations. Bell *et al.* [15] extended the Engquist–Osher flux to the general system of conservation laws which may lose strict hyperbolicity and exhibit local linear degeneracies. Zachary and Colella [17] applied the extension to one-dimensional ideal MHD equations, and Zachary *et al.* [18] further extended the scheme to multidimensional situations. Dai and Woodward [20] extended the PPM to multidimensional ideal MHD equations on the base of an iterative Riemann solver. There is no doubt about that Riemann solvers for systems of conservation laws may have sophisticated uses, and Riemann solvers are always desired. But, for the use of a Riemann solver in a Godunov scheme, it is not necessary to calculate the full solution of a Riemann problem. It is important for a Godunov scheme that how only the necessary part of Riemann solution may be obtained if a Riemann problem is not fully solved. In this direction, Davis [21] developed simplified second-order Godunov methods on the base of an approximate Riemann solution.

The purpose of this paper is to develop a simple approximate Riemann solver for its use in high-order Godunov schemes for hyperbolic systems of conservation laws. A high-order scheme incorporated with the simple Riemann solver will be described in detail in this paper. The scheme will be tested through numerical examples involving strong shocks in Euler and ideal MHD equations. The correctness of the scheme will be shown through the comparison with the PPM and through the comparison with exact solutions of Riemann problems. The robustness of the scheme will be demonstrated through shock-tube problems.

The plan of this paper is as follows. In the second section, hyperbolic systems of conservation laws and Godunov schemes

0021-9991/95 $12.00

for the hyperbolic systems will be introduced. A simple Riemann solver and a high-order Godunov scheme will be introduced in the third section. Numerical examples for Euler and ideal MHD equations are provided in the fourth section. The conclusions of this paper and a brief discussion for Godunov schemes may be found in the last section of the paper.

2. CONSERVATION LAWS AND GODUNOV SCHEMES

Let us consider a hyperbolic system of conservation laws:

$$\frac{\partial \mathbf{U}}{\partial t} + \frac{\partial \mathbf{F}(\mathbf{U})}{\partial x} = 0. \tag{1}$$

Here $\mathbf{U}$ is a vector consisting of n variables $\mathbf{U} \equiv (u_1, u_2, ..., u_n)^T$, and $\mathbf{F}(\mathbf{U})$ is a flux vector $\mathbf{F}(\mathbf{U}) \equiv (f_1(\mathbf{U}), f_2(\mathbf{U}), ..., f_n(\mathbf{U}))^T$, where the superscript ^{T} stands for transpose. We define a matrix $\mathbf{A}(\mathbf{U})$ $(\equiv\{a_{jk}, j, k = 1, 2, ..., n\})$ by $a_{jk} \equiv \partial f_j(\mathbf{U})/\partial u_k$. The eigenvalues of the matrix $\mathbf{A}(\mathbf{U})$ denoted by c_k $(k = 1, 2, ..., n)$ are speeds of characteristic waves. We assume that an entropy wave (if it exists) has a zero characteristic speed, and each of the other characteristic speeds is either non-negative or non-positive; i.e., we will work on a Lagrangian coordinate.

The system is strictly hyperbolic if all characteristic speeds c_k $(k = 1, 2, ..., n)$ are real and distinct. Otherwise, it is nonstrictly hyperbolic. For example, Euler equations form a strictly hyperbolic system with characteristic speeds $-C_s$, 0, and C_s. Here C_s is the sound wave speed. Ideal MHD equations form a non-strictly hyperbolic system with characteristic speeds $-C_f$, $-C_a$, $-C_s$, 0, C_s, C_a, and C_f. Here C_f, C_a, and C_s are fast, Alfven, and slow wave speeds. When x-component of the magnetic field is zero, C_s and C_a vanishes. When both y- and z-components of the magnetic field vanish, either C_f or C_s is equal to C_a.

In this paper we will develop a simple Riemann solver for its use in high-order Godunov schemes for Eq. (1). Suppose we have a zone $x_i < x < x_{i+1}$ in a numerical grid. A Godunov scheme for Eq. (1) may be viewed as the following difference equation:

$$\langle \mathbf{U}(\Delta t)\rangle_i = \langle \mathbf{U}(0)\rangle_i + \frac{\Delta t}{\Delta x_i}(\overline{\mathbf{F}}_i - \overline{\mathbf{F}}_{i+1}). \tag{2}$$

Here Δt is the time step and Δx_i is the width of the zone, $\langle \mathbf{U}(t)\rangle_i$ is the average of $\mathbf{U}$ over the zone at time t, and $\overline{\mathbf{F}}_i$ is the time-averaged flux at x_i, i.e.,

$$\langle \mathbf{U}(t)\rangle_i \equiv \frac{1}{\Delta x_i}\int_{x_i}^{x_{i+1}} \mathbf{U}(t, x)\, dx, \tag{2a}$$

$$\overline{\mathbf{F}}_i \equiv \frac{1}{\Delta t}\int_0^{\Delta t} \mathbf{F}[\mathbf{U}(t, x_i)]\, dt. \tag{2b}$$

The difference equation (2) is exact and it may be obtained by integrating Eq. (1) over the rectangular $x_i < x < x_{i+1}$ and $0 < t < \Delta t$ in $(x - t)$-space. Thus the key ingredient of a Godunov scheme is the calculation of the time-averaged flux at interfaces of numerical zones for a given initial condition.

3. RIEMANN SOLVER AND NUMERICAL SCHEME

In this paper, the calculation for the time-averaged flux needed in a Godunov scheme is based on the characteristic formulations. The characteristic formulations for a hyperbolic system of conservation laws may be found in many standard textbooks (e.g., [22]).

For a given system, Eq. (1), consisting of n conservation laws, there are n characteristic waves. Suppose that c_k is speed of the kth characteristic wave and $\mathbf{L}_k(\mathbf{U})$ $(\equiv\{\alpha_{kj}(\mathbf{U}), j = 1, 2, ..., n\})$ is its associate left eigenvector of $\mathbf{A}(\mathbf{U})$, i.e.,

$$\mathbf{L}_k(\mathbf{U})\mathbf{A}(\mathbf{U}) = c_k(\mathbf{U})\mathbf{L}_k(\mathbf{U}).$$

We multiply Eq. (1) by the vector $\mathbf{L}_k^T(\mathbf{U})$ from the left and have

$$\mathbf{L}_k^T(\mathbf{U})\left[\frac{\partial \mathbf{U}}{\partial t} + c_k(\mathbf{U})\frac{\partial \mathbf{U}}{\partial x}\right] = 0.$$

Along the characteristic curve determined by $dx = c_k(\mathbf{U})\, dt$, we have

$$d\mathbf{U} = \left[\frac{\partial \mathbf{U}}{\partial t} + c_k(\mathbf{U})\frac{\partial \mathbf{U}}{\partial x}\right] dt.$$

From the last two equations, we have

$$\mathbf{L}_k^T(\mathbf{U})\, d\mathbf{U} = 0$$

along the characteristic curve. Thus we obtain the differential of the Riemann invariant for the kth characteristic wave:

$$dR_k \equiv \mathbf{L}_k^T(\mathbf{U})\, d\mathbf{U}.$$

Since c_k may be any one among n characteristic speeds of the system, The differentials of n Riemann invariants may be written as

$$dR_k \equiv \sum_{j=1}^{j=n} \alpha_{kj}(\mathbf{U})\, du_j \quad \text{for } k = 1, 2, ..., n. \tag{3}$$

Before we discuss the nonstrict hyperbolicity, we assume that Eq. (1) forms a strictly hyperbolic system. This assumption will be removed later. Let us consider a Riemann problem of the system. The high-order accuracy of the scheme will be introduced in the discussion for the numerical procedure in a

computer code later. A Riemann problem is an initial-value problem, Eq. (1), subject to a specific initial condition:

$$\mathbf{U}(x, t = 0) = \begin{cases} \mathbf{U}_L & (x < 0), \\ \mathbf{U}_R & (x > 0). \end{cases}$$

Here $\mathbf{U}_L$ and $\mathbf{U}_R$ are two constant states.

For a given set of initial states, $\mathbf{U}_L$ and $\mathbf{U}_R$, we calculate the time-averaged flux through the approximation $\overline{\mathbf{F}} = \mathbf{F}(\overline{\mathbf{U}})$, where $\overline{\mathbf{U}}$ is the solution of the following set of linear equations ($k = 1, 2, ..., n$):

$$\overline{\mathbf{L}}_k^T(\overline{\mathbf{U}} - \mathbf{U}_R) = 0 \quad \text{for all } k \text{ with } c_k < 0. \tag{4a}$$

$$\overline{\mathbf{L}}_k^T(\overline{\mathbf{U}} - \mathbf{U}_L) = 0 \quad \text{for all } k \text{ with } c_k > 0. \tag{4b}$$

$$\overline{\mathbf{L}}_{k_0}^T(\overline{\mathbf{U}} - \mathbf{U}_0) = 0 \quad \text{for } c_{k_0}(\mathbf{U}) = 0. \tag{4c}$$

Here

$$\mathbf{U}_0 \equiv \tfrac{1}{2}(\mathbf{U}_L + \mathbf{U}_R), \tag{5a}$$

$$\overline{\mathbf{L}}_k \equiv \tfrac{1}{2}\,\text{sign}[\mathbf{D}_k(\mathbf{U}_R)][\text{abs}(\mathbf{L}_k(\mathbf{U}_L)) + \text{abs}(\mathbf{L}_k(\mathbf{U}_R))] \quad \text{for } c_k < 0, \tag{5b}$$

$$\overline{\mathbf{L}}_k \equiv \tfrac{1}{2}\,\text{sign}[\mathbf{D}_k(\mathbf{U}_L)][\text{abs}(\mathbf{L}_k(\mathbf{U}_L)) + \text{abs}(\mathbf{L}_k(\mathbf{U}_R))] \quad \text{for } c_k > 0. \tag{5c}$$

Here $\mathbf{D}_k(\mathbf{U})$ ($\equiv\{d_{ij}, i, j = 1, 2, ..., n\}$) is a diagonal matrix with d_{jj} equal to the jth element of vector $\mathbf{L}_k(\mathbf{U})$; sign($\mathbf{D}_k$) is defined as a diagonal matrix whose elements are the signs of elements of $\mathbf{D}_k$, and function abs($\mathbf{L}$) is defined as a vector whose elements are absolute values of elements of the vector $\mathbf{L}$. Actually, the jth component of vector $\overline{\mathbf{L}}_k$ is obtained by summing absolute values of the jth component of left and right vectors, $\mathbf{L}_k(\mathbf{U}_L)$ and $\mathbf{L}_k(\mathbf{U}_R)$, and by adjusting its sign to match the sign of the jth component of the left or right vector, depending on the propagation direction of the characteristic wave.

Equations (4a), (4b), (4c) come from the invariance of Riemann invariants along their characteristic curves. For the coefficients (i.e., the elements of $\overline{\mathbf{L}}_k$) in the set of linear Eqs. (4a), (4b), we have proposed formulations Eqs. (5b), (5c) instead of normal algebraic averages. The dependence of the vector $\overline{\mathbf{L}}_k$ on the propagation directions (i.e., the sign of c_k) of characteristic waves in Eqs. (5b), (5c) comes from the consideration of upwind nature, and summation of absolute values is introduced for the robustness of the solver. The strategy is necessary for a general system, although it is not for some of them. The coefficients in differentials of Riemann invariants, i.e., the elements of $\mathbf{L}_k$, are functions of the state $\mathbf{U}$. According to our experience in simulations for Euler and MHD equations, the more obvious average $(\mathbf{U}_L + \mathbf{U}_R)/2$ does not work for strong shocks unless more sophisticated Riemann solvers are introduced. For example, a coefficient in differentials of Riemann invariants for MHD equations may be proportional to B_y. Here B_y is the y-component of the magnetic field. If $B_{yL} = -B_{yR}$, the more obvious average without the function abs will make the coefficient vanishing. Vanishing coefficients in differentials of Riemann invariants will cause the set of linear Eqs. (4a), (4b) singular, although each component of the magnetic field at both left and right states does not vanish. Numerical tests for a variety of shock-tube problems involving strong hydrodynamical and MHD shocks shows that the average procedure, Eqs. (5b), (5c), works quite well, as will be seen later.

We mention that the consideration for the higher-order accuracy of the scheme may be reached through the replacement of the left and right states, $\mathbf{U}_L$ and $\mathbf{U}_R$, in Eqs. (4a), (4b) by corresponding domain-averages, and $\mathbf{U}_0$ in Eq. (4c) by the point value after an interpolation. The interpolation and the domain-averages will be introduced later. We should point out that Eqs. (4a), (4b) are decoupled from Eq. (4c) in the Lagrangian coordinate for many systems, such as Euler and ideal MHD equations.

For a system losing the strict hyperbolicity, eigenvalues $c_k(\mathbf{U})$ ($k = 1, 2, ..., n$) may become degenerate at some state $\mathbf{U}^*$. Mathematically, the degeneracy may cause a singularity when the set of linear Eqs. (4a)–(4c) is solved. To physically remove the degeneracy requires a more complete set of equations than conservation laws themselves. Our principle is to use a simple approach to remove the degeneracy under the condition that the approximation introduced by the approach does not influence numerical results. If the eigenvalues become degenerate at $\mathbf{U} = \mathbf{U}^*$, we will replace the local $\mathbf{U}$ by $(\mathbf{U}^* + \varepsilon)$ when we calculate the flux through Eqs. (4a)–(4c). Here ε is a vector with small values for its elements. The ε should be sufficient small but within the accuracy of digits of an actual machine. The influence of the artificial ε on numerical results is negligible because ε is very small. Actual values of ε may depend on a specific system of conservation laws.

For a given initial value problem and a numerical grid, our scheme starts from a set of zone-averages of conserved quantities. Cubic polynomials are used to interpolate each element of the vector $\mathbf{U}$ to find the values of the element at interfaces of numerical zones. For a uniform grid, the value of the vector $\mathbf{U}$ at the left interface; i.e., x_i, of the ith zone, $\mathbf{U}_{i,L}$, is found to be

$$\mathbf{U}_{i,L} = \langle \mathbf{U} \rangle_{i-1} + \tfrac{1}{2}(\langle \mathbf{U} \rangle_i - \langle \mathbf{U} \rangle_{i-1}) - \tfrac{1}{6}(\Delta \mathbf{U}_i - \Delta \mathbf{U}_{i-1}). \tag{6a}$$

Here $\Delta \mathbf{U}_i$ is the difference across the ith zone which is defined as

$$\Delta \mathbf{U}_i \equiv \tfrac{1}{2}(\langle \mathbf{U} \rangle_{i+1} - \langle \mathbf{U} \rangle_{i-1}).$$

For a nonuniform grid, the value at the interface is

$$\mathbf{U}_{i,L} = \langle \mathbf{U} \rangle_{i-1} + f_a(\langle \mathbf{U} \rangle_i - \langle \mathbf{U} \rangle_{i-1}) + f_{da}\Delta \mathbf{U}_i + f_{dal}\Delta \mathbf{U}_{i-1}. \tag{6b}$$

Here $\Delta\mathbf{U}_i$ is the difference of the variable across the ith zone for the nonuniform grid which is defined as

$$\Delta\mathbf{U}_i \equiv g_{dal}(\langle\mathbf{U}\rangle_i - \langle\mathbf{U}\rangle_{i-1}) + g_{dar}(\langle\mathbf{U}\rangle_{i+1} - \langle\mathbf{U}\rangle_i),$$

and f_a, f_{da}, f_{dal}, g_{dal}, and g_{dar} are geometry factors related to the nonuniform grid, which have forms:

$$g_{dal} = \Delta x_i(2\Delta x_{i+1} + \Delta x_i)/[\Delta x_{i-1} + \Delta x_i)(\Delta x_{i+1} + \Delta x_i + \Delta x_{i-1})],$$

$$g_{dar} = \Delta x_i(2\Delta x_{i-1} + \Delta x_i)/[\Delta x_i + \Delta x_{i+1})(\Delta x_{i+1} + \Delta x_i + \Delta x_{i-1})],$$

$$f_{da} = -\Delta x_{i-1}(\Delta x_{i-2} + \Delta x_{i-1})/[2\Delta x_{i-1} + \Delta x_i) \times (\Delta x_{i-2} + \Delta x_{i-1} + \Delta x_i + \Delta x_{i+1})],$$

$$f_{dal} = \Delta x_i(\Delta x_i + \Delta x_{i+1})/[(2\Delta x_i + \Delta x_{i-1}) \times (\Delta x_{i-2} + \Delta x_{i-1} + \Delta x_i + \Delta x_{i+1})],$$

$$f_a = [\Delta x_{i-1} - 2(\Delta x_i f_{da} + \Delta x_{i-1} f_{dal})]/(\Delta x_{i-1} + \Delta x_i).$$

After we get the values of the vector $\mathbf{U}$ at interfaces, the monotonicity constraint originally suggested by Van Leer [5] is applied to these values at interfaces. As we know, interpolated structures are not always monotone increasing (decreasing) even though they have been constructed from monotone data. Over- and undershoots in interpolated internal zone structures eventually give rise to over- and undershoots in zone-averaged data. Van Leer realized that an advection scheme may be made to preserve the monotonicity of its initial data if any nonmonotone interpolated zone structures are flattened so that they become monotone. This leads the Van Leer's monotonicity constraint: no values interpolated within a zone shall lie outside the range defined by the zone averages for this zone and its two neighbors.

We assume that $\mathbf{U}(x, t)$ is continuous inside each zone but may have big jumps across an interface of two neighboring zones. After the monotonicity constraint is applied, we have three values of $\mathbf{U}$ for each numerical zone: a zone-average $\langle\mathbf{U}\rangle_i$ and the values at two interfaces of the zone, $\mathbf{U}_{i,L}$ and $\mathbf{U}_{i,R}$. A parabola defined by these three values is used to interpolate the structure of $\mathbf{U}$ inside the zone for the calculation of domain-averages. The parabola has the form

$$\mathbf{U}_i^{(p)}(\xi) = \mathbf{U}_{i,L}(1 - \xi) + \mathbf{U}_{i,R}\xi + \mathbf{U}_{i,6}(1 - \xi)\xi. \tag{7}$$

Here ξ is the distance to the left interface and $\mathbf{U}_{i,6}$ is defined as

$$\mathbf{U}_{i,6} \equiv 6\langle\mathbf{U}\rangle_i - 3(\mathbf{U}_{i,L} + \mathbf{U}_{i,R}).$$

Different waves have different domains of dependence. For the interface between the $(i-1)$th and ith zones, i.e., x_i, the domain-average for the kth wave is defined as

$$\langle\mathbf{U}\rangle_{d,k} \equiv \frac{1}{x_i - x_{dk}}\int_{x_{dk}}^{x_i} \mathbf{U}(0, x)\,dx \quad \text{for either } c_k > 0 \text{ or } c_k < 0.$$

Here $x_{dk} \equiv x_i - c_k\,dt$ for either case. For the parabolic interpolation, the domain-average of $\mathbf{U}$ is found to be

$$\langle\mathbf{U}\rangle_{d,k} = \mathbf{U}_{i-1,R} - \tfrac{1}{2}\sigma_{i-1,k}[\mathbf{U}_{i-1,R} - \mathbf{U}_{i-1,L} - \mathbf{U}_{i-1,6}(1 - \tfrac{2}{3}\sigma_{i-1,k}) \quad \text{for } c_k > 0, \tag{8a}$$

$$\langle\mathbf{U}\rangle_{d,k} = \mathbf{U}_{i,L} + \tfrac{1}{2}\sigma_{i,k}[\mathbf{U}_{i,R} - \mathbf{U}_{i,L} + \mathbf{U}_{i,6}(1 - \tfrac{2}{3}\sigma_{i,k})] \quad \text{for } c_k < 0. \tag{8b}$$

Here $\sigma_{i,k}$ is the Courant number $|c_k|\,\Delta t/\Delta x_i$.

After domain-averages are obtained, Eqs. (4a)–(4c) are modified to reach a higher-order accuracy for the flux $\bar{\mathbf{F}}$ needed in the Godunov scheme:

$$\bar{\mathbf{L}}_k^T(\bar{\mathbf{U}} - \langle\mathbf{U}\rangle_{d,k}) = 0 \quad \text{for all } k \text{ with } c_k \neq 0,$$

$$\bar{\mathbf{L}}_{k_0}^T(\bar{\mathbf{U}} - \mathbf{U}_{i,L}) = 0 \quad \text{for } c_{k_0} = 0.$$

Here $\langle\mathbf{U}\rangle_{d,k}$ is the domain-average corresponding to the characteristic speed c_k, and it is calculated through Eq. (8a) if $c_k > 0$, otherwise it is calculated through Eq. (8b). $\bar{\mathbf{L}}_k$ is defined as

$$\bar{\mathbf{L}}_k \equiv \tfrac{1}{2}\text{sign}[\mathbf{D}_k(\langle\mathbf{U}\rangle_{i-1})][\text{abs}(\mathbf{L}_k(\langle\mathbf{U}\rangle_{i-1})) + \text{abs}(\mathbf{L}_k(\langle\mathbf{U}\rangle_i))] \quad \text{for } c_k > 0,$$

$$\bar{\mathbf{L}}_k \equiv \tfrac{1}{2}\text{sign}[\mathbf{D}_k(\langle\mathbf{U}\rangle_i)][\text{abs}(\mathbf{L}_k(\langle\mathbf{U}\rangle_{i-1})) + \text{abs}(\mathbf{L}_k(\langle\mathbf{U}\rangle_i))] \quad \text{for } c_k < 0,$$

$$\bar{\mathbf{L}}_{k_0} \equiv \tfrac{1}{2}[\mathbf{L}_{k_0}(\langle\mathbf{U}\rangle_{i-1}) + \mathbf{L}_{k_0}(\langle\mathbf{U}\rangle_i)].$$

After obtaining the flux, we update the conserved quantity $\mathbf{U}$, according to Eq. (2), by adding the flux advected into and subtracting the flux advected out from a zone during a time step.

If a transformation on original physical equations has been made to make the speed of the entropy wave vanish, it is normally desired to map the conserved quantities from a Lagrangian grid to the Euler grid after the dynamical step described above. Suppose a Lagrangian grid is denoted by $x_i^{(l)}$ $(i = 1, 2, \ldots, N+1)$. As described before, cubic polynomials are used to interpolate $\mathbf{U}$ in order to find the values at interfaces of numerical zones. The monotonicity constraint is used to adjust the values at the interface. A parabola is used for the structure inside a zone for each physical variable in order to perform the mapping.

For the mapping, we have to find the conserved quantity in a zone (x_i, x_{i+1}) of the Eulerian grid:

$$\int_{x_i}^{x_{i+1}} \mathbf{U}(x)\,dx.$$

Note that a zone in the Eulerian grid (x_i, x_{i+1}) may extend to several zones in the Lagrangian grid. The contribution of a zone in the Lagrangian grid, which is completely covered by the domain (x_i, x_{i+1}), to the integral is simply the product of

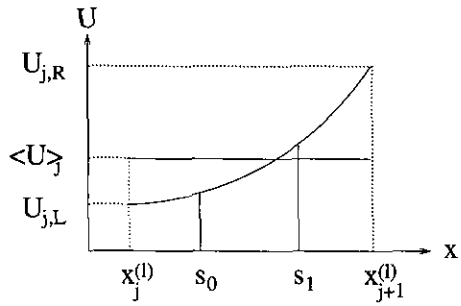

FIG. 1. Illustration for a integral needed in the mapping from the Lagrangian to Eulerian grids. $x_j^{(l)}$ is an interface in the Lagrangian grid, $\langle \mathbf{U} \rangle_j$ is a zone-average, and $\mathbf{U}_{j,L}$ and $\mathbf{U}_{j,R}$ are two values at two interfaces.

the zone-average and the width of the zone. For those zones in the Lagrangian grid which are partially covered by the domain (x_i, x_{i+1}), we have to find an integral

$$\int_{s_0}^{s_1} \mathbf{U}(x)\, dx.$$

Here (s_0, s_1) is a part of a zone $(x_j^{(l)}, x_{j+1}^{(l)})$, as shown in Fig. 1. From the parabolic interpolation Eq. (7), the integral is found to be

$$\int_{s_0}^{s_1} \mathbf{U}(x)\, dx = (s_1 - s_0)[\mathbf{U}_{j,L} + \tfrac{1}{2}(\mathbf{U}_{j,6} + \mathbf{U}_{j,R} - \mathbf{U}_{j,L})(\xi_j + \eta_j) - \tfrac{1}{3}\mathbf{U}_{j,6}(\xi_j^2 + \xi_j \eta_j + \eta_j^2)].$$

Here ξ_j and η_j are defined as

$$\xi_j \equiv (s_1 - x_j^{(l)})/(x_{j+1}^{(l)} - x_j^{(l)}),$$
$$\eta_j \equiv (s_0 - x_j^{(l)})/(x_{j+1}^{(l)} - x_j^{(l)}).$$

4. NUMERICAL EXAMPLES

In this section, we will apply the principles described in the last section to Euler and ideal MHD equations. The set of Euler equations is strictly hyperbolic, while the set of ideal MHD equations is not.

4.1. *Euler Equations*

One-dimensional Euler equations are [24]

$$\frac{\partial \rho}{\partial t} + \frac{\partial}{\partial x}(\rho u) = 0,$$

$$\frac{\partial}{\partial t}(\rho u) + \frac{\partial}{\partial x}(\rho u^2 + p) = 0,$$

$$\frac{\partial}{\partial t}(\rho E) + \frac{\partial}{\partial x}[u(\rho E + p)] = 0.$$

Here ρ is the mass density, u the flow velocity, p the thermal pressure, E the total specific energy defined by $E \equiv \varepsilon + 1/2\, u^2$ with ε the specific internal energy. Thermal pressure is related to the internal energy through the gamma-law equation of state $p = (\gamma - 1)\rho\varepsilon$ with γ being the ratio of specific heat capacities.

Euler equations may be rewritten in a Lagrangian mass coordinate defined by $dm \equiv \rho\, dx$:

$$\frac{\partial \mathbf{U}}{\partial t} + \frac{\partial \mathbf{F}(\mathbf{U})}{\partial m} = 0 \tag{9}$$

with

$$\mathbf{U} \equiv \begin{bmatrix} V \\ u \\ E \end{bmatrix}, \quad \mathbf{F}(\mathbf{U}) \equiv \begin{bmatrix} -u \\ p \\ pu \end{bmatrix}.$$

Here $V \equiv 1/\rho$. The characteristic speeds, C_0 for an entropy wave and $C_{s\pm}$ for two sound waves, of Eqs. (9) are

$$C_0 = 0, \quad C_{s\pm} = \pm\sqrt{\gamma p \rho}.$$

The differentials of their associated Riemann invariants are

$$dR_0 = d(p/\rho^\gamma),$$
$$dR_\pm = dp + C_{s\pm}\, du.$$

We give four numerical examples for Euler equations: the steepening of a sound wave, the propagation of a shock, the Sod problem, and a shock-tube problem involving two shocks. Two hundred uniform numerical zones between zero and unity are used, and γ is set to 1.4 in the Sod problem and $\frac{5}{3}$ in the others. An artificial viscosity as in the PPM is used in the second and forth examples. In Figs. 2–5 for the four examples, the dashed lines are initial conditions and the dotted lines are the results of our simulations. The dotted lines in these figures are hidden by the solid lines, which are the results obtained by the PPM without the steepener for contact discontinuities.

For the steepening of a sound wave, we initially set a sound wave through dR_+:

$$\frac{dR_+}{dx} = -0.5(2\pi)\cos(2\pi x),$$

$$\frac{dR_0}{dx} = \frac{dR_-}{dx} \equiv 0.$$

The initial conditions for ρ, p, and u are obtained by solving the set of ordinary differential equations and values (1, 1, -1.28) for (ρ, p, u) at $x = 0$. Figure 2 shows the results at $t = 1$ and 2. It may be seen that the sound wave has become

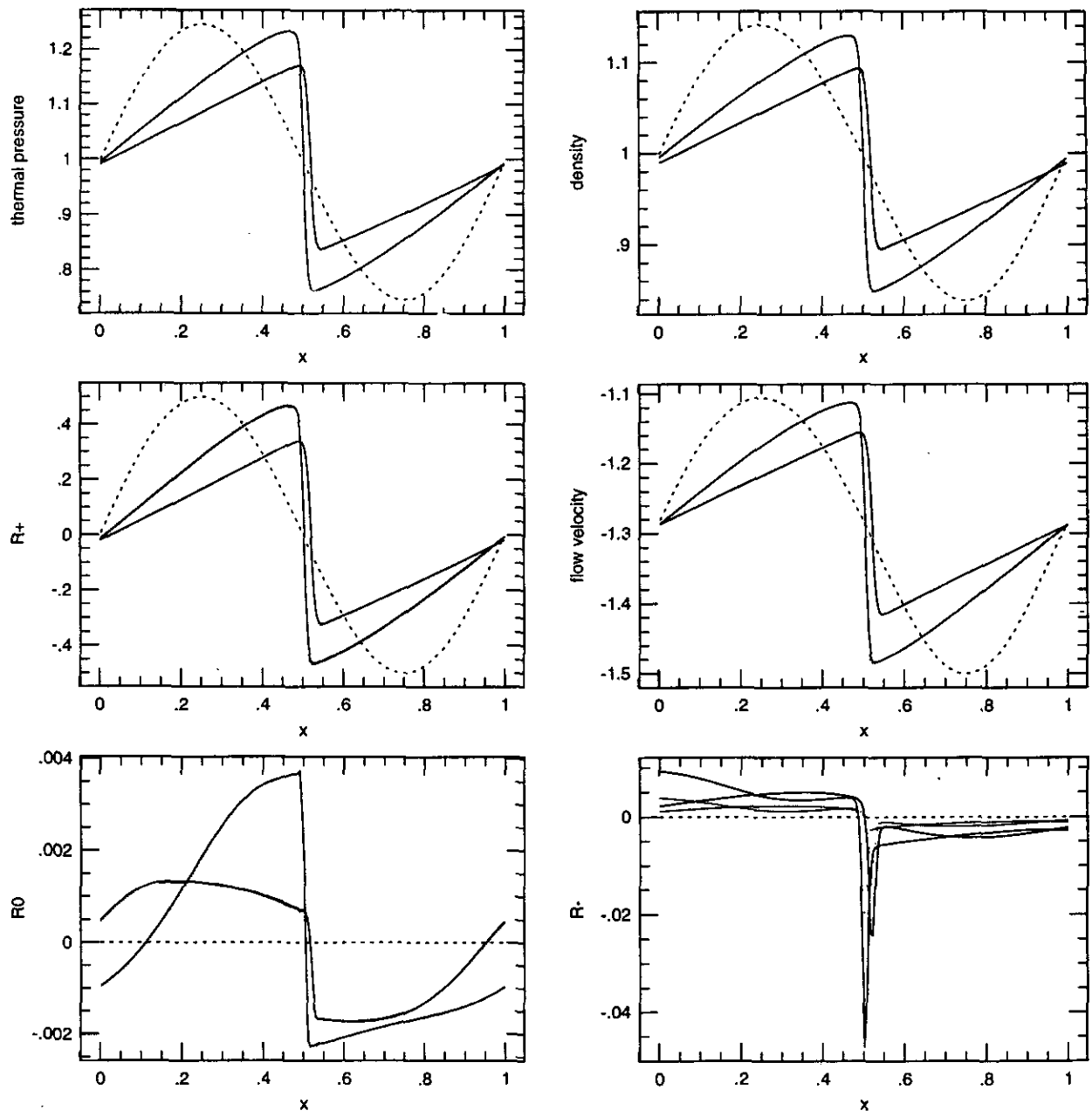

FIG. 2. The steepening of a sound wave, 200 zones, no artificial viscosity. The dashed lines are the initial condition. Other two profiles for each variable are the results at $t = 1.0$ and 2.0, at which the wave traveled about one and two wavelengths, respectively. The solid lines are obtained from the PPM code, and the dotted lines, which are hidden by solid lines, are the results from our scheme.

a shock in $t = 1$, and the scheme correctly simulated the steepening and the propagation of the wave. Note that the dotted lines are completely hidden by the solid lines, except in the profiles for R_0. Riemann invariants plotted in the figure are meaningless across the shock since Riemann invariants are defined for smooth flow. The non-constant behavior in smooth regions for R_- and R_0 is the numerical error. In Fig. 3, a shock with a Mach number 60 is used to test the correctness of the scheme for the propagation of shocks. We initially set $(\rho, p, u) = (3.99666, 449.975, 0)$ for $x < 0.1$ and $(1, 0.1, -18.3661)$ for $x > 0.1$. The results at $t = 0.12$ are shown in the figure. The Sod problem has the initial condition: $(\rho, p, u) = (1, 1, 0)$ for $x < 0.5$ and $(0.125, 0.1, 0)$ for $x > 0.5$. The results of the problem at $t = 0.14$ are shown in Fig. 4. The correctness of the results may be justified through the comparison with the results in [4]. In order to test the interaction between shocks,

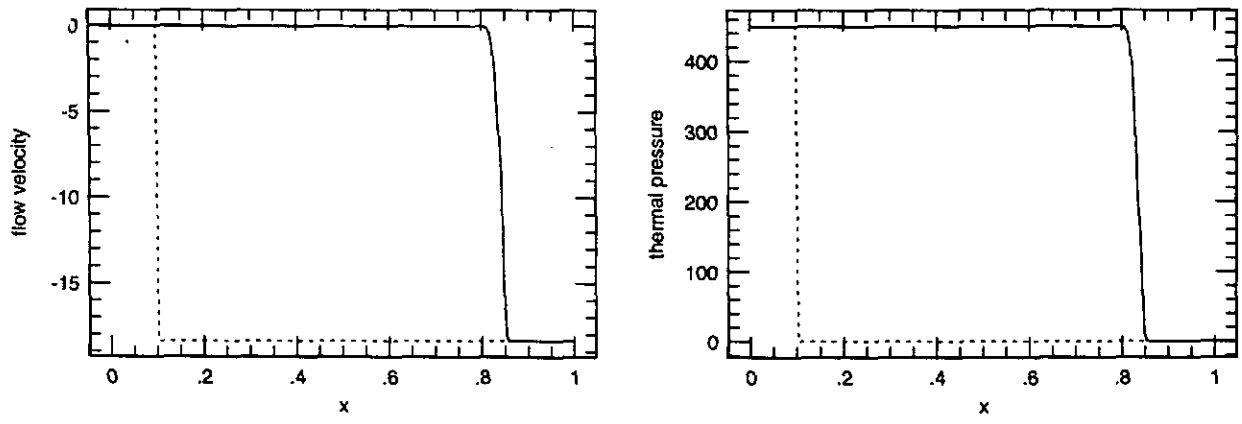

FIG. 3. The propagation of a shock with a Mach number 60 with an artificial viscosity, 200 zones. The dashed lines are the initial condition. The solid lines are obtained from the PPM code, and the dotted lines which are completely hidden by solid lines, are the results from our scheme at $t = 0.12$.

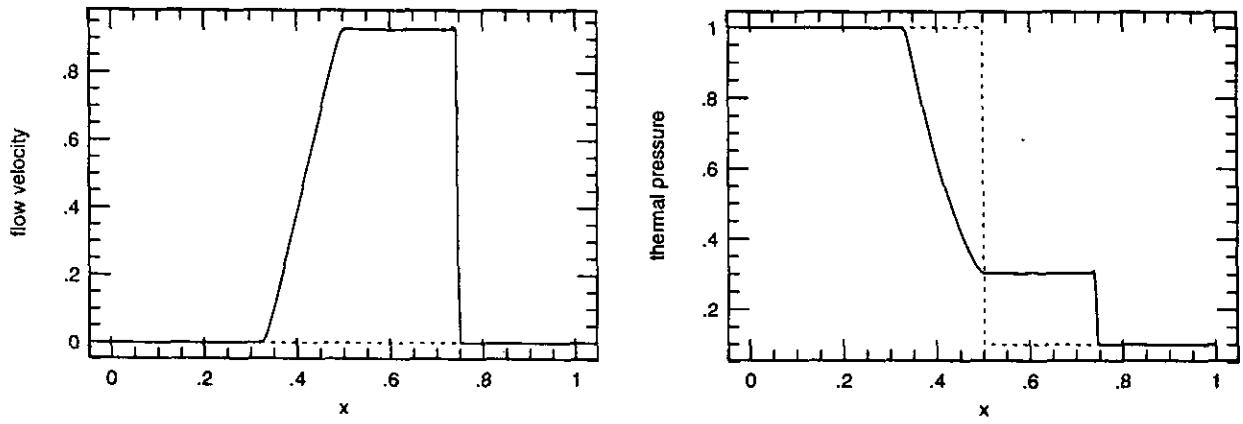

FIG. 4. The Sod problem, 200 zones, no artificial viscosity. The dashed lines are the initial condition. The solid lines are obtained form the PPM code, and the dotted lines which are completely hidden by solid lines, are the results from our scheme at $t = 0.14$.

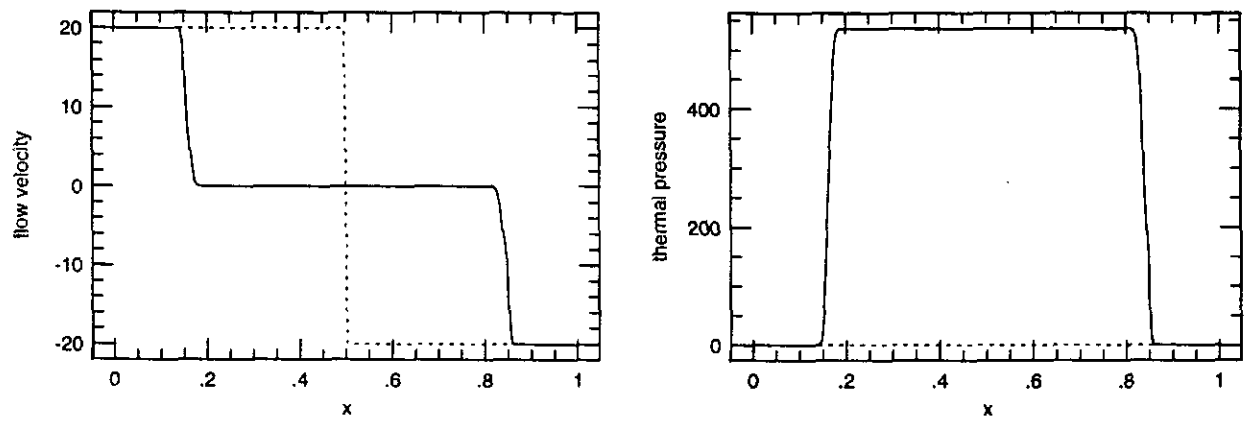

FIG. 5. A shock tube problem in Euler equations with an artificial viscosity, 200 zones. The dashed lines are the initial condition. The solid lines are obtained from the PPM code, and the dotted lines which are completely hidden by solid lines, are the results from our scheme at t = 0.05. The emanating shocks have a Mach number about 20 each.

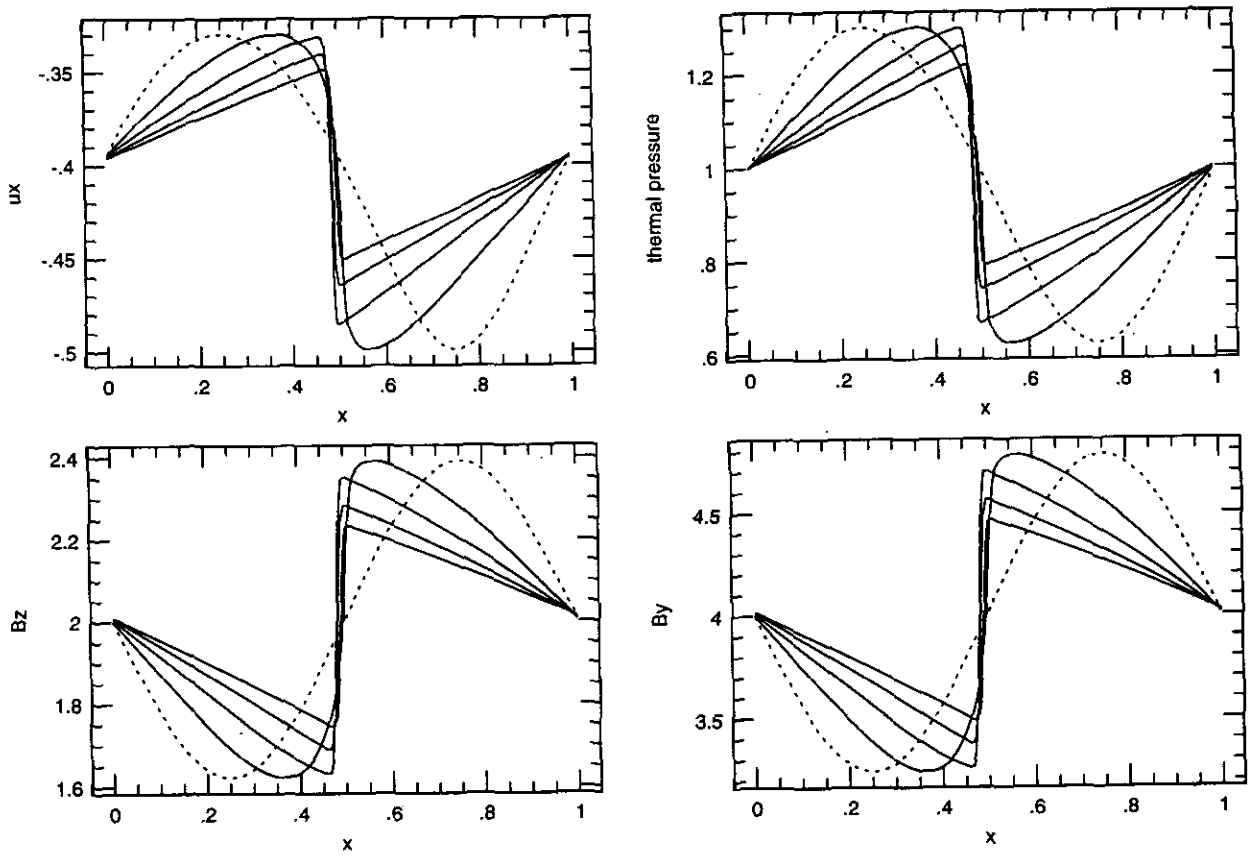

FIG. 6. The steepening of a slow wave in ideal MHD equations without any artificial viscosity, 200 zones, $B_x = 2$. The dashed lines are initial profiles, and the wave speed c_s at $x = 0$ for the initial condition is about 0.4 The time interval between two consecutive profiles is 1.27, during which the wave travels about a half wavelength.

we set a shock-tube problem with the initial condition: $(\rho, p, u) = (1, 1, 20)$ for $x < 0.5$ and $(1, 1, -20)$ for $x > 0.5$. Our results for the shock-tube problem at $t = 0.05$ are shown in the Fig. 5. The exact solution of the corresponding Riemann problem is not difficult to find, which contains two shocks with a Mach number about 20.7 each.

4.2. *Ideal Magnetohydrodynamical Equations*

One-dimensional ideal MHD equations have the form [24]:

$$\frac{\partial \rho}{\partial t} + \frac{\partial}{\partial x}(\rho u_x) = 0,$$

$$\frac{\partial}{\partial t}(\rho u_x) + \frac{\partial}{\partial x}(\rho u_x^2 + P) = 0,$$

$$\frac{\partial}{\partial t}(\rho u_y) + \frac{\partial}{\partial x}(\rho u_x u_y + \Lambda_y) = 0,$$

$$\frac{\partial}{\partial t}(\rho u_z) + \frac{\partial}{\partial x}(\rho u_x u_z + \Lambda_z) = 0,$$

$$\frac{\partial}{\partial t}(\rho E) + \frac{\partial}{\partial x}(\rho u_x E + u_x P + u_y \Lambda_y + u_z \Lambda_z) = 0,$$

$$\frac{\partial B_y}{\partial t} - \frac{\partial}{\partial x}(u_y B_x - u_x B_y) = 0,$$

$$\frac{\partial B_z}{\partial t} - \frac{\partial}{\partial x}(u_z B_x - u_x B_z) = 0.$$

Here ρ is the mass density, (u_x, u_y, u_z) and (B_x, B_y, B_z) are three components of the flow velocity and the magnetic field. B_x is constant. E is the specific total energy, P, Λ_y, and Λ_z are the diagonal and off-diagonal total pressure. E, P, Λ_y, and Λ_z are defined as

$$E \equiv \varepsilon + \frac{1}{2}(u_x^2 + u_y^2 + u_z^2) + \frac{1}{8\pi\rho}(B_x^2 + B_y^2 + B_z^2),$$

$$P \equiv p + \frac{1}{8\pi}(B_y^2 + B_z^2 - B_x^2),$$

$$\Lambda_y \equiv -\frac{1}{4\pi} B_x B_y,$$

$$\Lambda_z \equiv -\frac{1}{4\pi} B_x B_z.$$

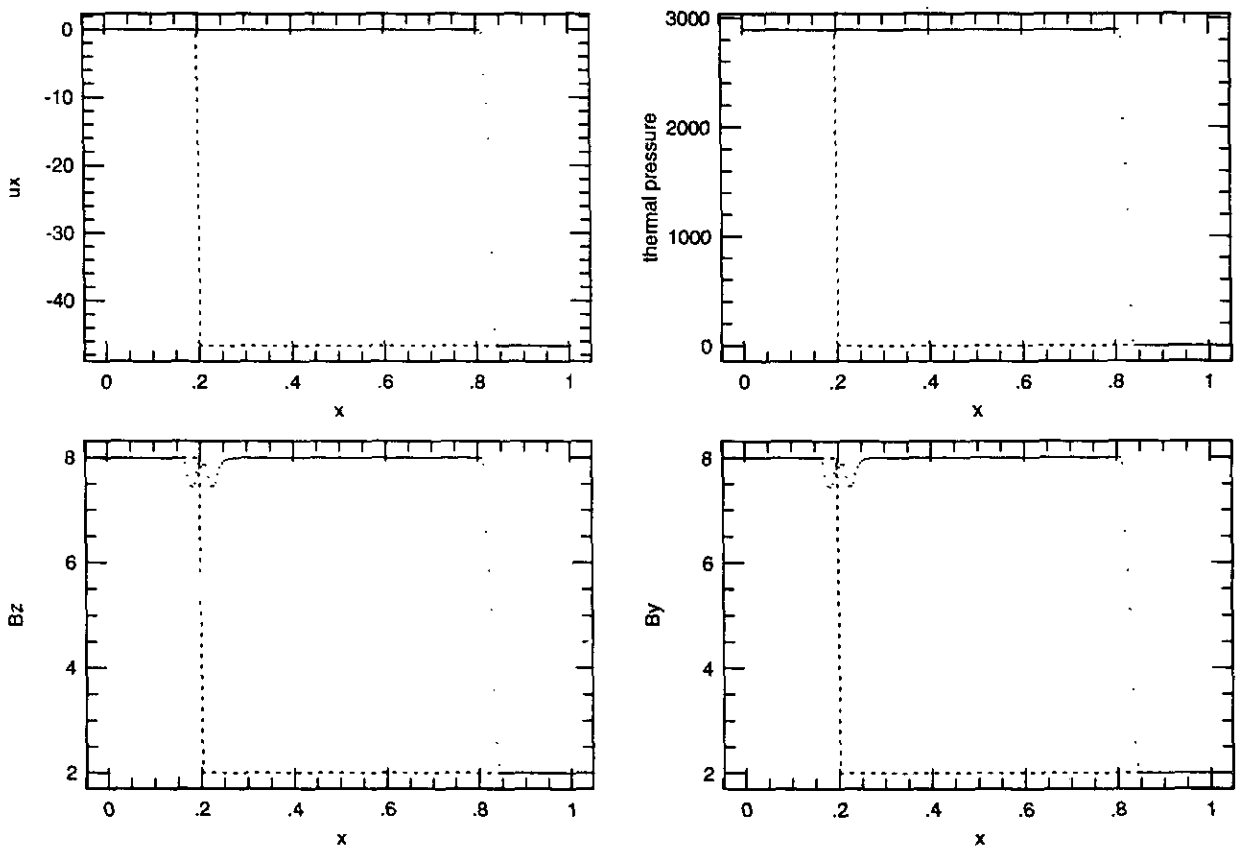

FIG. 7. The propagation of a fast shock with a Mach number 60 in ideal MHD equations with an artificial viscosity, 200 zones, $B_x = 4$. The dashed lines are the initial condition, and the dotted lines are the results at t = 0.04. The structures near x = 0 in B_y and B_z are due to the pure discontinuities used in the initial condition, and they may be reduced by a small internal structure in the initial condition.

with ε the specific internal energy density and p the thermal pressure. The gamma-law equation of state is assumed in our simulation. As for Euler equations, the dynamical step is carried out in a Lagrangian grid followed by a mapping operation from the Lagrangian to Eulerian grids. Thus we rewrite ideal MHD equations in a Lagrangian mass coordinate ($dm \equiv \rho\, dx$):

$$\frac{\partial \mathbf{U}}{\partial t} + \frac{\partial \mathbf{F}(\mathbf{U})}{\partial m} = 0 \tag{10a}$$

with

$$U \equiv \begin{bmatrix} V \\ u_x \\ u_y \\ u_z \\ VB_y \\ VB_z \\ E \end{bmatrix}, \quad \mathbf{F}(\mathbf{U}) \equiv \begin{bmatrix} -u_x \\ P \\ \Lambda_y \\ \Lambda_z \\ -B_x u_y \\ -B_x u_z \\ Pu_x + \Lambda_y u_y + \Lambda_z u_z \end{bmatrix}. \tag{10b}$$

Following the procedure in Section 3, it is easy to find characteristic speeds of Eq. (10a), which are two fast wave speeds $C_{f\pm}$, two Afiven wave speeds $C_{a\pm}$, two slow wave speeds $C_{s\pm}$, and a vanishing entropy wave speed:

$$C_{fs}^2 = \tfrac{1}{2}[(C_0^2 + C_a^2 + C_t^2) \pm \sqrt{(C_0^2 + C_a^2 + C_t^2)^2 - 4C_0^2C_a^2}].$$

Here C_0, C_a, and C_t are defined as

$$C_0 \equiv \sqrt{\gamma p \rho},$$
$$C_a \equiv \sqrt{\rho B_x^2/4\pi},$$
$$C_t \equiv \sqrt{\rho(B_y^2 + B_z^2)/4\pi}.$$

The differentials of their associated Riemann invariants are

$$dR_{f\pm} \equiv (C_f^2 - C_a^2)(dP \pm C_f du_x) + \rho\Lambda_y(d\Lambda_y \pm C_f du_y) + \rho\Lambda_z(d\Lambda_z \pm C_f du_z),$$

$$dR_{s\pm} \equiv (C_s^2 - C_a^2)(dP \pm C_s du_x) + \rho\Lambda_y(d\Lambda_y \pm C_s du_y) + \rho\Lambda_z(d\Lambda_z \pm C_s du_z),$$

$$dR_{a\pm} \equiv \pm C_a(B_z du_y - B_y du_z) - \frac{1}{4\pi} B_x(B_z dB_y - B_y dB_z).$$

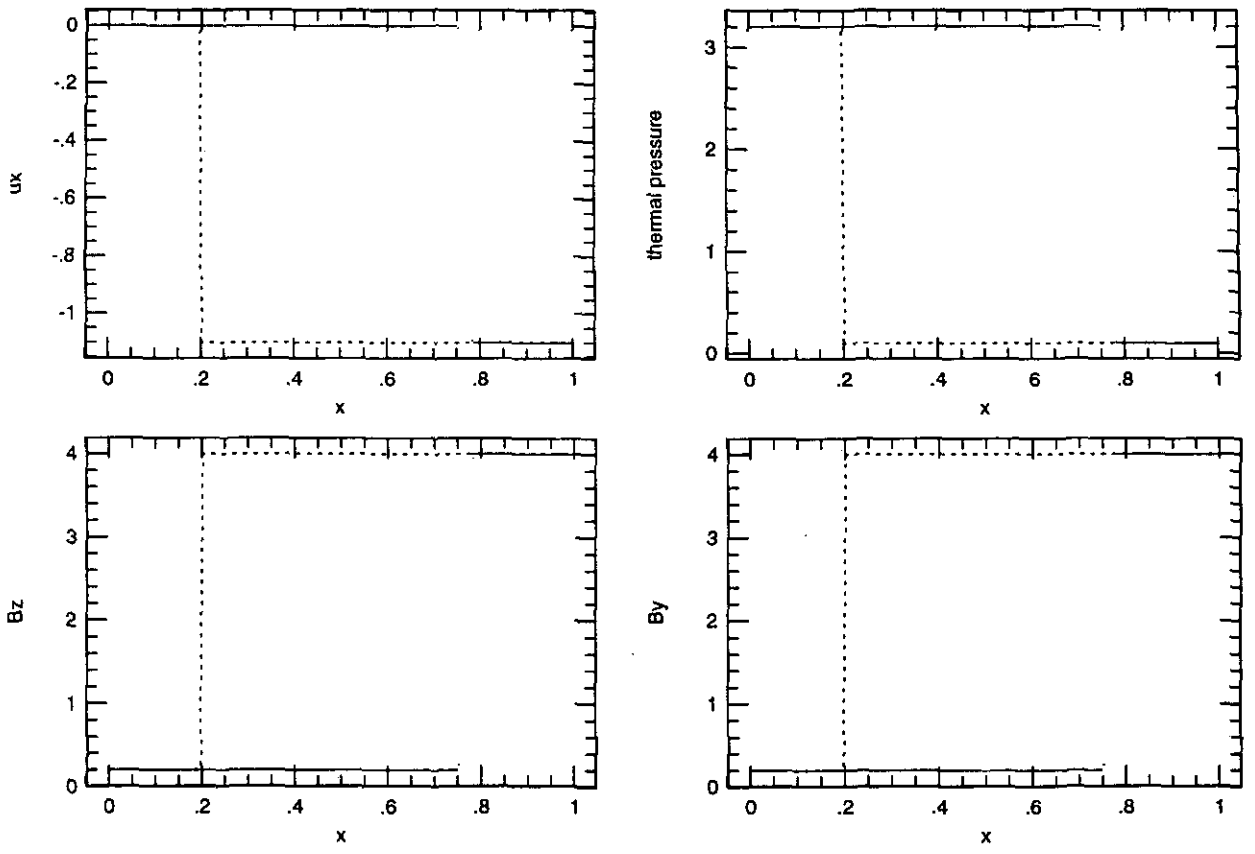

FIG. 8. The propagation of a slow shock with a Mach number 5.6 in ideal MHD equations with an artificial viscosity. 200 zones, $B_x = 6$. The dashed lines are the initial profiles, and the dotted lines are the results at t = 1.0.

The vanishing of B_x of (B_y, B_z) may cause degenerate of MHD waves. Mathematically, the degeneracy will cause a singularity when Eqs. (4a)–(4c) are solved. As discussed in Section 3 for the time-averaged flux needed in a Godunov scheme, a component of the magnetic field is set to a small value if it is close to zero. Since the artificial value is very small compared with the thermal pressure but is within the accuracy of digits of a machine, the numerical influence of the artificial value on the system is negligible. In our simulations, the artificial value is such chosen that the corresponding magnetic pressure is 0.001% of the local thermal pressure.

In order to show the correctness of the scheme incorporated with the Riemann solver for ideal MHD equations, we give six numerical examples involving discontinuities, in which γ is set to $\frac{5}{3}$. The first example is for the steepening of a slow wave. Initially a slow wave is set up through a set of Riemann invariants,

$$\frac{dR_{s+}}{dx} = -0.2(2\pi)\cos(2\pi x),$$

$$\frac{dR_{s-}}{dx} = \frac{dR_{f\mp}}{dx} = \frac{dR_{a\pm}}{dx} \equiv 0$$

with $B_x = 2$. The initial condition for normal physical variables is obtained through solving the set of ordinary differential equations defined by these Riemann invariants and values (1, 1, −0.393771, 0, 0, 4, 2) for $(\rho, p, u_x, u_y, u_z, B_y, B_z)$ at $x = 0$. Two hundred numerical zones are used. Initially, the slow wave speed at $x = 0$ is about 0.4. The steepening of the wave is shown by five profiles in Fig. 6 which correspond to $t = 0$ (dashed lines), 1.27, 2.54, 3.81, and 5.08. Since the flow move to the negative x-direction, the shock developed is nearly stationary, which is the worst case for the text.

The second example is to test the propagation of a fast shock. Initially the fast shock is $(\rho, p, u_x, u_y, u_z, B_y, B_z)$ = (3.99650, 2891.26, 0, −0.01535, −0.01535, 7.99498, 7.99498) for $x <$ 0.2, and (1, 0.1, −46.5973, 0, 0, 2, 2) for $x > 0.2$ with $B_x =$ 4, as shown by dashed lines in Fig. 7. The Mach number of the shock is about 60. Two hundred zones are used. The profiles at $t = 0.04$ are shown by the dots in the figure. The structure near $x = 0.2$ in the magnetic field is due to the pure discontinuity used in the initial condition, which is referred to as the "starting error" and may be reduced if we give the initial shock a small internal structure [20]. It may be seen in our numerical results that the propagation of the shock is quite stable. The third

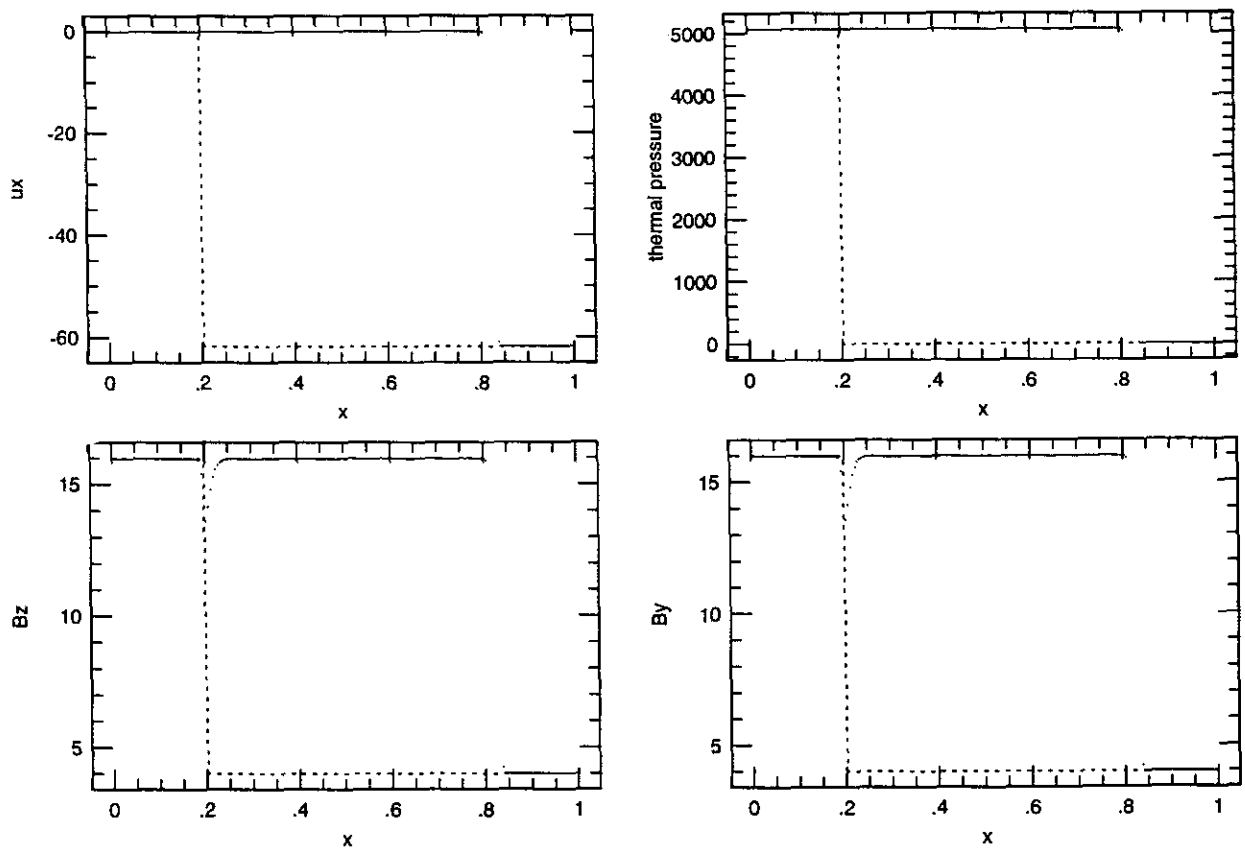

FIG. 9. The propagation of a magnetosonic shock with a Mach number 50 in ideal MHD equations with an artificial viscosity, 200 zones, $B_x = 0$. The dashed lines are the initial condition, and the dotted lines are the results at t = 0.03. The structures near x = 0 in B_x and B_y are due to the pure discontinuities used in the initial condition, and they may be reduced by a small internal structure in the initial condition.

TABLE I

A Solution for the Riemann Problem Shown in Fig. 10

Regions	ρ	p	ux	uy	uz	By	Bz
L	1.011E + 00	9.447E − 01	1.470E + 01	3.677E + 00	3.677E + 00	4.044E + 00	4.044E + 00
A	3.882E + 00	2.770E + 02	2.252E − 02	3.862E + 00	3.862E + 00	1.567E + 01	1.567E + 01
B	4.041E + 00	2.964E + 02	1.599E − 05	1.838E + 00	1.838E + 00	1.567E + 00	1.567E + 00
C	3.882E + 00	2.770E + 02	−2.247E − 02	−1.864E − 01	−1.864E − 01	1.567E + 01	1.567E + 01
R	1.000E + 00	1.000E − 01	−1.483E + 01	0.000E + 00	0.000E + 00	4.000E + 00	4.000E + 00

Note. $B_x = 4$, $\gamma = \frac{5}{3}$.

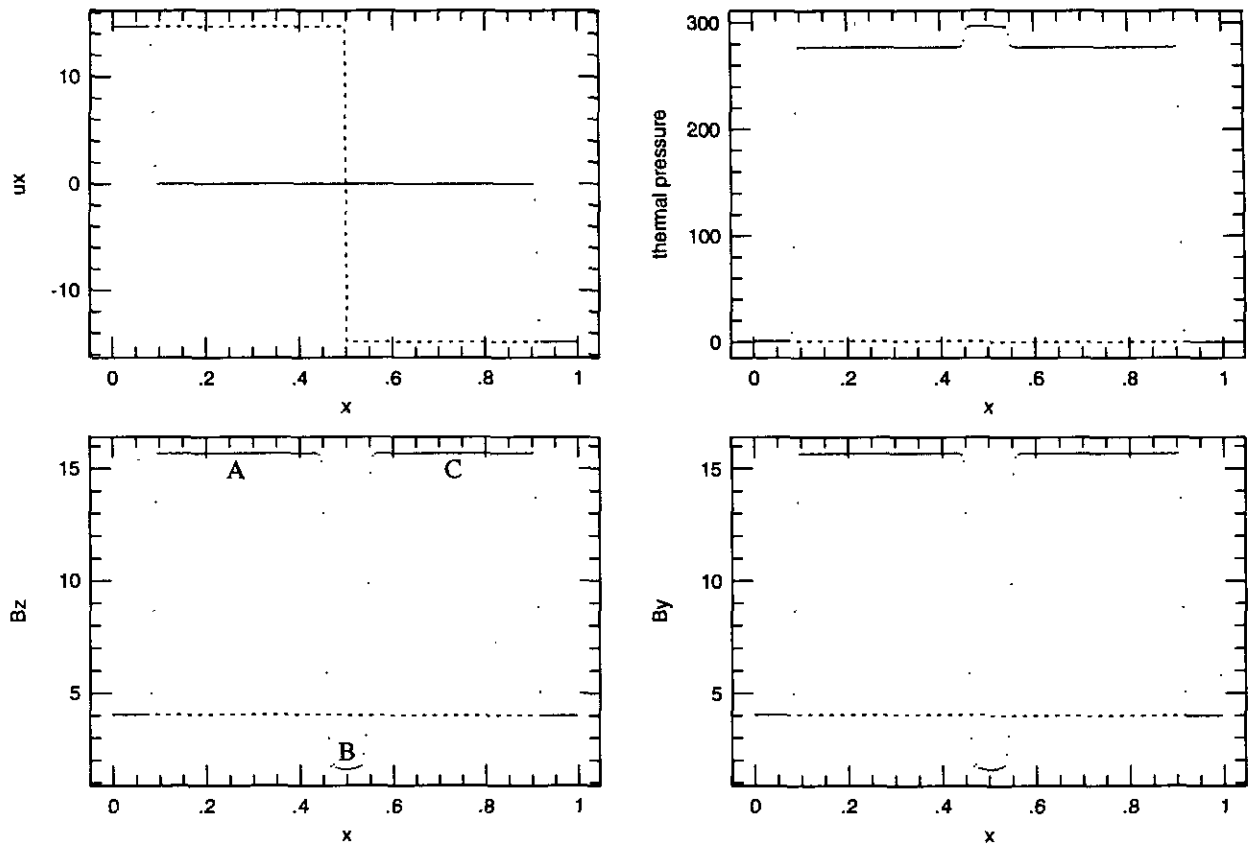

FIG. 10. A shock tube problem in ideal MHD equations with an artificial viscosity, 200 zones, $B_x = 4$. The dashed lines are the initial condition, and the dotted lines are the results at t = 0.08. The two emanating fast shocks have Mach numbers about 10 and 8.9, and the slow shocks have a Mach number 1.04 each. The exact solution of the constant states in different regions is shown in the Table I which contains the solution of the corresponding Riemann problem.

TABLE II

A Solution for the Riemann Problem in Fig. 11

Regions	ρ	p	ux	uy	uz	By	Bz
L	1.844E − 01	1.337E − 01	4.341E + 00	3.147E + 00	4.726E − 01	2.128E + 00	1.064E + 00
A	3.903E − 01	1.413E + 00	9.888E − 01	5.006E + 00	1.402E + 00	7.600E + 00	3.800E + 00
B	3.903E − 01	1.413E + 00	9.888E − 01	2.787E + 00	3.326E + 00	2.687E + 00	8.061E + 00
C	7.261E − 01	4.996E + 00	−4.768E − 07	1.762E + 00	2.501E − 01	5.374E − 01	1.612E + 00
D	4.034E − 01	4.996E + 00	−4.768E − 07	1.762E + 00	2.501E − 01	5.374E − 01	1.612E + 00
E	2.168E − 01	1.413E + 00	−1.327E + 00	3.864E − 01	−3.877E + 00	2.687E + 00	8.061E + 00
F	2.168E − 01	1.413E + 00	−1.327E + 00	−2.590E + 00	−1.295E + 00	7.600E + 00	3.800E + 00
R	1.000E − 01	1.000E − 01	−5.961E + 00	0.000E + 00	0.000E + 00	2.000E + 00	1.000E + 00

Note. $B_x = 5$, $\gamma = \frac{5}{3}$.

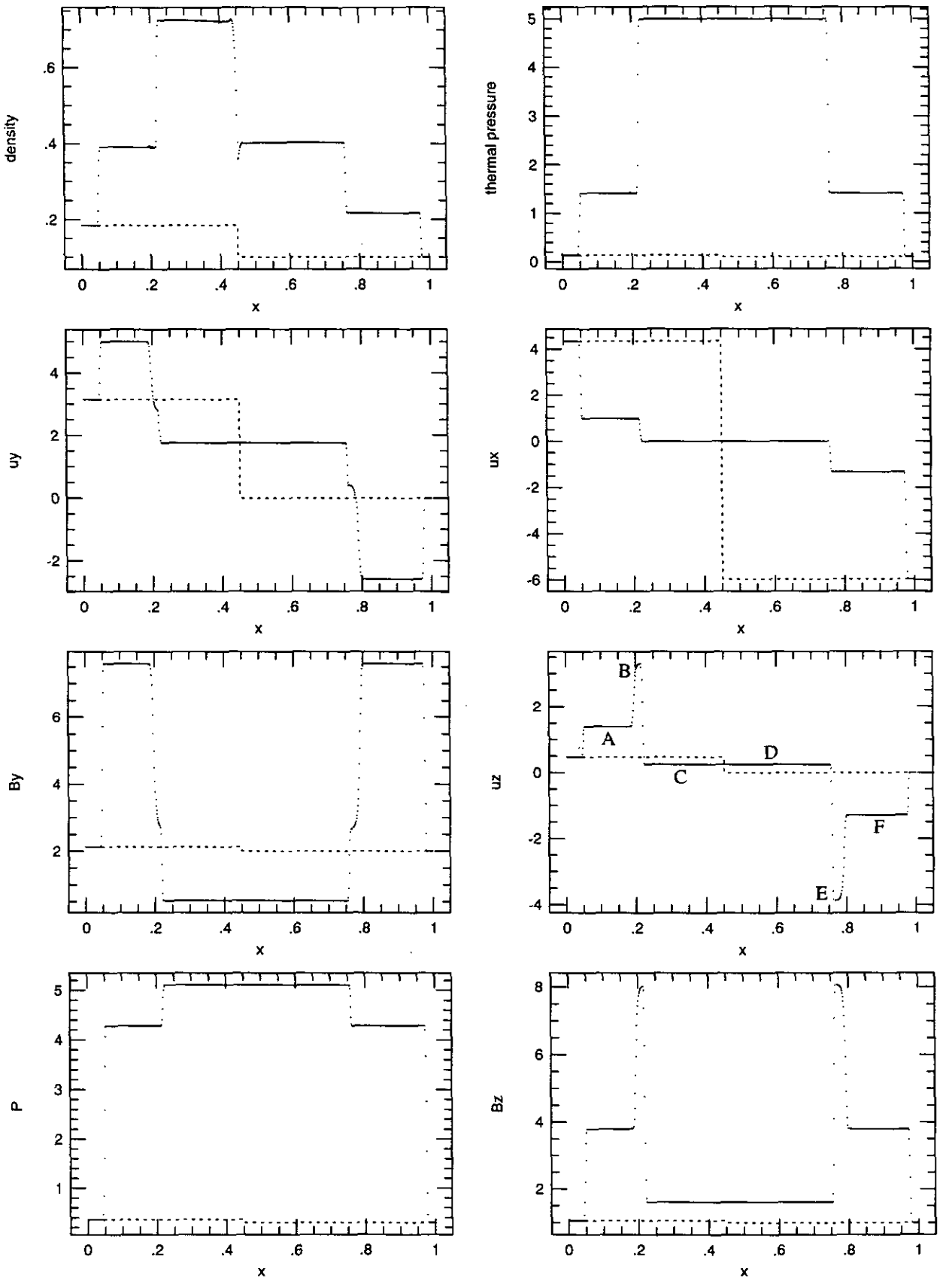

FIG. 11. A shock tube problem in ideal MHD equations with an artificial viscosity, 400 zones, $B_x = 5$. The dashed lines are the initial profiles, and the dotted lines are the results at t = 0.2. Two fast shocks, two slow shocks, two rotational discontinuities, and one contact discontinuity are emanated. The exact solution for the constant states in different regions is shown in Table II which contains the solution of the corresponding Riemann problem.

example is to test the propagation of a slow shock. As is well known, the Mach number for a slow shock is limited by the Alfven wave speed in its preshock state. A strong slow shock may be set up if we give a relative large B_x. We initially give a slow shock shown by the dashed lines in Fig. 8: $(\rho, p, u_x, u_y, u_z, B_y, B_z) = (2.95828, 3.20260, 0, 1.09047, 1.09047, 0.2, 0.2)$ for $x < 0.2$; $(1, 0.1, -1.10140, 0, 0, 4, 4)$ for $x > 0.2$ with $B_x = 6$. The Mach number for the slow shock is about 5.6. The dots in the figure show the profiles at $t = 1.0$.

As we mentioned before, we use the general characteristic formulations even for degenerate situations. The fourth example for the propagation of a magnetosonic shock with a Mach number 50 is to show the correctness of the approximation. The initial condition is shown by the dashed lines in Fig. 9: $(\rho, p, u_x, u_y, u_z, B_y, B_z) = (3.99295, 5065.49, 0, 0, 0, 15.9718, 15.9718)$ for $x < 0.2$; $(1, 0.1, -61.7339, 0, 0, 4, 4)$ for $x > 0.2$. The results at t = 0.03 are shown by the dots in the figure. Again the structure near x = 0 in the magnetic field is the starting error resulting from the pure discontinuity in the initial condition.

The remaining two examples are shock-tube problems involving multiple discontinuities. The first shock-tube problem is that $(\rho, p, u_x, u_y, u_z, B_y, B_z) = (1.01071, 0.944733, 14.6972, 3.67709, 3.67709, 4.04358, 4.04358)$ for $x < 0.5$ and $(1, 0.1, 14.825, 0, 0, 4, 4)$ for $x > 0.5$ with $B_x = 4$, as shown by the dashed lines in Fig. 10. The results at $t = 0.08$ are shown by the dots in the figure. Two fast shocks with Mach numbers 8.9 and 10.1, and two slow shocks are generated from the initial discontinuity. Table I gives the exact solution of the corresponding Riemann problem in the different constant regions indicated by A, B, and C, which are obtained by a Riemann solver [19] through enough iterations. The correctness of the scheme may be justified through the comparison between the figure and table.

The second shock tube problem is for an initial condition which will emanate seven discontinuities. The initial condition is $(\rho, p, u_x, u_y, u_z, B_y, B_z) = (0.184364, 0.133743, 4.34106, 3.14725, 4.72569, 2.128, 1.064)$ for $x < 0.45$ and $(0.1, 0.1, -5.96134, 0, 0, 2, 1)$ for $x > 0.45$ with $B_x = 5$, which is shown by dashed lines in Fig. 11. In order to display the structure between the slow shocks and the rotational discontinuities involved in this problem, 400 numerical zones are used. The dots in the figure show the results at $t = 0.2$. The exact solution of the corresponding Riemann problem is shown in Table II, which contains two fast shocks with Mach numbers 1.73 and 1.75, two slow shocks with a Mach number 1.91 each, two rotational discontinuities with a rotated angle 45° each, and one contact discontinuity.

5. CONCLUSIONS AND DISCUSSIONS

A simple approximate Riemann solver for its use in high-order Godunov schemes for hyperbolic systems of conservation laws has been developed. The solver is based on characteristic formulations. The procedure of a high-order Godunov scheme incorporated with the Riemann solver is described in detail for one-dimensional hyperbolic systems of conservation laws. The scheme is illustrated through Euler and ideal MHD equations. The steepening of hydrodynamical and MHD waves, the propagation of hydrodynamical and MHD shocks, and shock-tube problems are tested as numerical examples. The correctness of the scheme incorporated with the Riemann solver has been shown through the comparison with PPM for Euler equations and through the comparison with exact solutions of Riemann problems for ideal MHD equations. The robustness of the scheme has been demonstrated through these examples which involve multiple discontinuities. It has been shown that the scheme incorporated with the Riemann solver offers the principle advantages of high-order Godunov schemes.

In this paper, we have not given the results for the numerical example studied by previous investigators [16, 19, 20] for compound waves in ideal MHD. We would like to mention that the scheme in this paper gives the same result as the previous investigations for this problem, which is actually the solution of the dissipative MHD equations. Like most schemes for hyperbolic systems of conservation laws, our scheme actually performs the simulation for dissipative equations because of the numerical dissipation which is intrinsically present in a numerical scheme for discontinuities. The numerical dissipation cannot be removed through refining the mesh for discontinuities.

ACKNOWLEDGMENTS

We acknowledge useful discussions with Thomas W. Jones. This work was supported by the U.S. Department of Energy through Grant DE-FG02-87ER25035, by the National Science Foundation under Grant ASC-9309829, by the Minnesota Supercomputer Institute, and by Army Research Office Contract DAALO3-89-C-0038 with Army High Performance Computing Research Center at the University of Minnesota.

REFERENCES

1. S. K. Godunov, *Math. Sb.* **47,** 271 (1959). [Russian]
2. P. D. Lax and B. Wendroff, *Commun. Pure Appl. Math.* **13,** 217 (1960).
3. P. D. Lax, *Hyperbolic Systems of Conservation Laws and Mathematical Theory of Shock Waves* (SIAM, Philadelphia, 1973).
4. G. Sod, *J. Comput. Phys.* **27,** 1 (1978).
5. B. Van Leer, *J. Comput. Phys.* **32,** 101 (1979).
6. P. L. Roe, *J. Comput. Phys.* **43,** 358 (1981).
7. B. Engquist and S. Osher, *Math. Comput.* **36,** 321 (1981).
8. P. R. Woodward and P. Colella, in *Lecture Notes in Physics*, Vol. 141 (Springer-Verlag, New York/Berlin, 1981). p. 434.
9. S. Osher and F. Solomon, *Math Comput.* **38,** 339 (1983).
10. A. Harten, *J. Comput. Phys.* **49,** 357 (1983).
11. P. Colella and P. R. Woodward, *J. Comput. Phys.* **54,** 174 (1984).
12. I. L. Chern, J. Glimm, O. McBryan, B. Plohr, and S. Yaniv, *J. Comput. Phys.* **62,** 83 (1986).
13. P. R. Woodward, in *Astrophysical Radiation Hydrodynamics*, edited by K.-H. A. Winkler and M. L. Norman (Reidel, Dordrecht, 1986), p. 245.

14. J. B. Bell, P. Colella, and J. A. Trangenstein, *J. Comput. Phys.* **82,** 362 (1989).

15. R. J. LeVeque, *Numerical Methods for Conservation Laws*, 2nd ed. (Birkhauser, Basel, 1992).

16. M. Brio and C. C. Wu, *J. Comput. Phys.* **75,** 400 (1988).

17. A. L. Zachary and P. Colella, *J. Comput. Phys.* **99,** 341 (1992).

18. A. L. Zachary, A. Malagoli, and P. Colella, *SIAM J. Sci. Comput.* **15,** 263 (1994).

19. W. Dai and P. R. Woodward, *J. Comput. Phys.* **111,** 354 (1994).

20. W. Dai and P. R. Woodward, *J. Comput. Phys.* **115,** 485 (1994).

21. S. F. Davis, *SIAM J. Sci. Stat. Comput.* **9,** 445 (1988).

22. R. Courant and K. O. Friedrichs, *Supersonic Flow an Shock Wave*, 5th ed. (Interscience, New York, 1967).

23. L. D. Landau and E. Lifshits, *Fluid Mechanics* (Pergamon, New York, 1959).

24. L. D. Landau and E. Lifshits, *Electrodynamics of Continuous Media* (Pergamon, New York, 1960).